Report

Stimulation of glycolysis promotes cardiomyocyte proliferation after injury in adult zebrafish

Ryuichi Fukuda[1,2,*] (ID), Rubén Marín-Juez[1,2,†], Hadil El-Sammak[1,2,†], Arica Beisaw[1,2], Radhan Ramadass[1,2], Carsten Kuenne[3], Stefan Guenther[3,4], Anne Konzer[2,5], Aditya M Bhagwat[2,5], Johannes Graumann[2,5] (ID) & Didier YR Stainier[1,2,**] (ID)

Abstract

Cardiac metabolism plays a crucial role in producing sufficient energy to sustain cardiac function. However, the role of metabolism in different aspects of cardiomyocyte regeneration remains unclear. Working with the adult zebrafish heart regeneration model, we first find an increase in the levels of mRNAs encoding enzymes regulating glucose and pyruvate metabolism, including pyruvate kinase M1/2 (Pkm) and pyruvate dehydrogenase kinases (Pdks), especially in tissues bordering the damaged area. We further find that impaired glycolysis decreases the number of proliferating cardiomyocytes following injury. These observations are supported by analyses using loss-of-function models for the metabolic regulators Pkma2 and peroxisome proliferator-activated receptor gamma coactivator 1 alpha. Cardiomyocyte-specific loss- and gain-of-function manipulations of pyruvate metabolism using Pdk3 as well as a catalytic subunit of the pyruvate dehydrogenase complex (PDC) reveal its importance in cardiomyocyte dedifferentiation and proliferation after injury. Furthermore, we find that PDK activity can modulate cell cycle progression and protrusive activity in mammalian cardiomyocytes in culture. Our findings reveal new roles for cardiac metabolism and the PDK-PDC axis in cardiomyocyte behavior following cardiac injury.

Introduction

Cardiac metabolism is essential to produce adenosine triphosphate (ATP), which is required for cardiac homeostasis and function (Neely & Morgan, 1974; Kolwicz *et al*, 2013). During development, embryonic cardiomyocytes (CMs) mainly utilize glucose metabolism for ATP production (Piquereau & Ventura-Clapier, 2018). As the heart grows, CMs exhibit metabolic changes and rely mostly on fatty acid oxidation (Cho *et al*, 2006; Chung *et al*, 2007, 2010; Kreipke *et al*, 2016). It has also been shown that under conditions of cardiac disease, such as ischemia and heart failure, CMs revert to glucose as an energy source (Das *et al*, 1987; Doenst *et al*, 2013).

Unlike adult mammals, adult zebrafish regenerate their heart effectively after injury (Poss *et al*, 2002). During cardiac regeneration, CMs re-express *hand2* (Schindler *et al*, 2014), a transcription factor gene required for cardiac development, as well as an embryonic myosin (Sallin *et al*, 2015), and they also exhibit sarcomere disassembly (Jopling *et al*, 2010; Ben-Yair *et al*, 2019; Beisaw *et al*, 2020). These and other studies (Kikuchi *et al*, 2010; Wu *et al*, 2016; Grajevskaja *et al*, 2018) suggest that in zebrafish, CMs undergo dedifferentiation to supply new CMs during cardiac regeneration. Thus, CMs may utilize similar regulatory mechanisms during development and regeneration, yet the role of cardiac metabolism in these processes remains unclear.

Pyruvate dehydrogenase kinase plays an essential role in pyruvate metabolism (Gudi *et al*, 1995; Takubo *et al*, 2013; Zhang *et al*, 2014). Glucose is initially converted to pyruvate through several glycolytic intermediates, and then, pyruvate is converted to lactate via anaerobic fermentation (Lehninger *et al*, 2005), or to acetyl-coenzyme A (acetyl-CoA) by the PDC (Behal *et al*, 1993). By inhibiting the conversion of pyruvate to acetyl-CoA, PDK induces the conversion of pyruvate to lactate, via anaerobic fermentation (Korotchkina & Patel, 2001; Koukourakis *et al*, 2005). These studies indicate that PDK regulates the shift of pyruvate metabolism between glycolysis and OXPHOS (Korotchkina & Patel, 2001; Koukourakis *et al*, 2005; Takubo *et al*, 2013; Park *et al*, 2018). Higher expression of PDKs in cancer and stem cells, which rely mainly on glycolysis, has been associated with their enhanced proliferation and migration (Takubo *et al*, 2013; Zhang *et al*, 2014; Park *et al*, 2018).

1 Department of Developmental Genetics, Max Planck Institute for Heart and Lung Research, Bad Nauheim, Germany
2 The German Centre for Cardiovascular Research (DZHK), Partner Site Rhine-Main, Max Planck Institute for Heart and Lung Research, Bad Nauheim, Germany
3 The Cardio-Pulmonary Institute (CPI) and Deep Sequencing Platform, Bad Nauheim, Germany
4 Bioinformatics and Deep Sequencing Platform, Max Planck Institute for Heart and Lung Research, Bad Nauheim, Germany
5 Biomolecular Mass Spectrometry, Max Planck Institute for Heart and Lung Research, Bad Nauheim, Germany
  *Corresponding author: Tel: +49 (0)6032 705 1302; E-mail: ryuichi.fukuda@mpi-bn.mspg.de
  **Corresponding author: Tel: +49 (0)6032 705 1332; E-mail: didier.stainier@mpi-bn.mpg.de
  †These authors contributed equally to this work

Here, we first show that glycolytic enzymes are upregulated at the transcriptional level during cardiac regeneration. Pharmacological and genetic manipulations as well as CM-specific modulation of glycolytic activity reveal its importance in CM proliferation after injury. We also found that modulation of pyruvate metabolism can affect mammalian CM cell cycle progression and cell behavior. Transcriptomic analyses show that PDK3 overexpression (OE) leads to higher levels of genes encoding cell cycle regulators in CMs. These data indicate that metabolism plays an important role in CM proliferation following cardiac injury.

Results and Discussion

Glycolysis and pyruvate metabolism modulate cardiomyocyte dedifferentiation and proliferation following cardiac injury

Adult mammalian CMs rely mainly on fatty acid oxidation as a source of energy (Cho *et al*, 2006; Chung *et al*, 2007, 2010; Kreipke *et al*, 2016). We started by performing proteomic analysis and found higher levels of fatty acid oxidation enzymes in adult zebrafish ventricles compared to those in juveniles (Fig 1A and B). These findings are consistent with mammalian models, in which adult CMs express higher levels of fatty acid oxidation enzymes (Puente *et al*, 2014; Fukushima *et al*, 2016).

It has been suggested that zebrafish CMs utilize similar regulatory mechanisms during cardiac development and regeneration (Poss *et al*, 2002; Jopling *et al*, 2010; Kikuchi *et al*, 2010; Wu *et al*, 2016). We have recently shown that glycolysis plays an important role during zebrafish cardiac development (Fukuda *et al*, 2019). Thus, we wanted to examine whether the expression levels of glycolytic enzyme genes were changed in zebrafish ventricles after cryoinjury. We found significant upregulation of many of them in the tissues bordering the damaged area when compared to remote areas (Fig 1C). This finding is supported by a single-cell RNA-sequencing analysis in regenerating zebrafish hearts (Honkoop *et al*, 2019). Notably, we found high upregulation of *pdk2b*, *pdk3b,* and *pdk4* (Fig 1C), which encode key enzymes that regulate pyruvate metabolism and promote glycolysis in a number of cell types including CMs (Zhao *et al*, 2008) and cancer cells (Koukourakis *et al*, 2005; Leclerc *et al*, 2017; Peng *et al*, 2018). We also measured lactate levels, which are indicative of glycolytic activity, and found higher levels in regenerating cardiac tissues (Fig EV1A). These and other observations (Honkoop *et al*, 2019) suggest that adult zebrafish CMs switch from fatty acid oxidation to glycolytic metabolism in response to cardiac injury. In order to examine the role of

glycolysis and Pdk function following cardiac injury, we treated zebrafish with 2-deoxy-D-glucose (2-DG) and dichloroacetate (DCA), which decrease glycolysis and Pdk function, respectively. Notably, these treatments led to a decrease in CM proliferation in the border zone following injury (Figs 1D and EV1B). We also found that the re-expression of embryonic myosin, which has been reported to indicate CM dedifferentiation during cardiac regeneration (Sallin *et al*, 2015), was reduced when glycolysis or Pdk function was decreased (Fig 1E). These data suggest that glycolysis and pyruvate metabolism as regulated by Pdk play a role in border zone CMs following cardiac injury.

Genetic manipulation of metabolic enzymes affects cardiomyocyte dedifferentiation and proliferation following cardiac injury

Next, we assessed whether the loss of specific metabolic enzymes affected CM behavior after cardiac injury. We first examined the role of Pkm2. Mammalian *Pkm* gives rise to two splice isoforms, *Pkm1* and *Pkm2*; PKM2 promotes glucose metabolism toward lactate, while PKM1 promotes glucose metabolism toward acetyl-CoA (Lehninger *et al*, 2005; Christofk *et al*, 2008). Knockdown of *PKM2* has been reported to lead to decreased glycolytic activity in human umbilical vein endothelial cells (Stone *et al*, 2018) and intestinal stem cells (Kim *et al*, 2019), as well as upregulation of PKM1 (Lunt *et al*, 2015; Zheng *et al*, 2016). Similarly, *Pkm2* OE in mouse CMs leads to enhanced glycolysis (Magadum *et al*, 2020). The zebrafish genome contains two *pkm* genes (*pkma* and *pkmb*), with *pkma* encoding both an orthologue of mammalian *Pkm1* (*pkma1*) and an orthologue of mammalian *Pkm2* (*pkma2*), while *pkmb* encodes another orthologue of mammalian *Pkm2* (Stone *et al*, 2018). Expression analysis in adult ventricles indicates that *pkma* is upregulated in tissues bordering the injured area, while *pkmb* is not (Fig 1C), suggesting a role for *pkma* following cardiac injury. In *pkma2* mutant zebrafish, the *pkma1* isoform, which promotes glucose metabolism toward acetyl-CoA, remains intact, suggesting that the metabolism of pyruvate to lactate is impaired while pyruvate oxidation is increased. These data indicate that a zebrafish *pkma2* mutant constitutes a potential model of impaired glycolysis, as pyruvate is expected to be converted preferentially to acetyl-CoA and not lactate. Thus, we examined $pkma2^{-/-}$; $pkmb^{+/-}$ animals, which do not display obvious cardiac defects compared to WT (Fig EV2A–C), and found that they exhibited a reduction in the number of proliferating CMs after cardiac injury (Figs 2A and EV2D). Consistently, the expression of embryonic myosin was also decreased in $pkma2^{-/-}$; $pkmb^{+/-}$ animals (Fig 2B). We also

---

Figure 1. Glycolysis and pyruvate metabolism play an important role following cardiac injury.

A   30 and 150 days post fertilization (dpf) zebrafish ventricles were isolated and relative protein levels determined (*n* = 3 biological replicates).

B   KEGG over-representation analysis for selected categories of upregulated proteins in 150 dpf hearts compared to 30 dpf hearts.

C   qPCR analysis of mRNA levels of glycolytic enzyme genes in 5 dpci remote and wound border cardiac tissue (*n* = 2–3 technical replicates using pooled cDNA from 10 ventricles for each condition (*n* = 2 for *pkmb* and *pdk4*, and *n* = 3 for the other genes).

D, E   Immunostaining of heart sections for PCNA and MEF2 (D) or N2.261 and MEF2 (E) in 5 dpci animals treated with PBS, 2-DG, or DCA; magnified view of area in white boxes shown below; white dashed lines outline the wound area; arrowheads point to PCNA⁺ (D) or N2.261⁺ (E) CMs; percentage of PCNA⁺ or N2.261⁺ CMs in the border zone shown on the right (*n* = 4–5 ventricles).

Data information: Error bars, s.e.m.; *P* values were calculated by Bayesian-moderated *t*-test (limma) (A, B), two-tailed unpaired *t*-test (C), or ordinary one-way ANOVA with Dunnett's multiple comparison test (D, E). Scale bars, 50 μm.
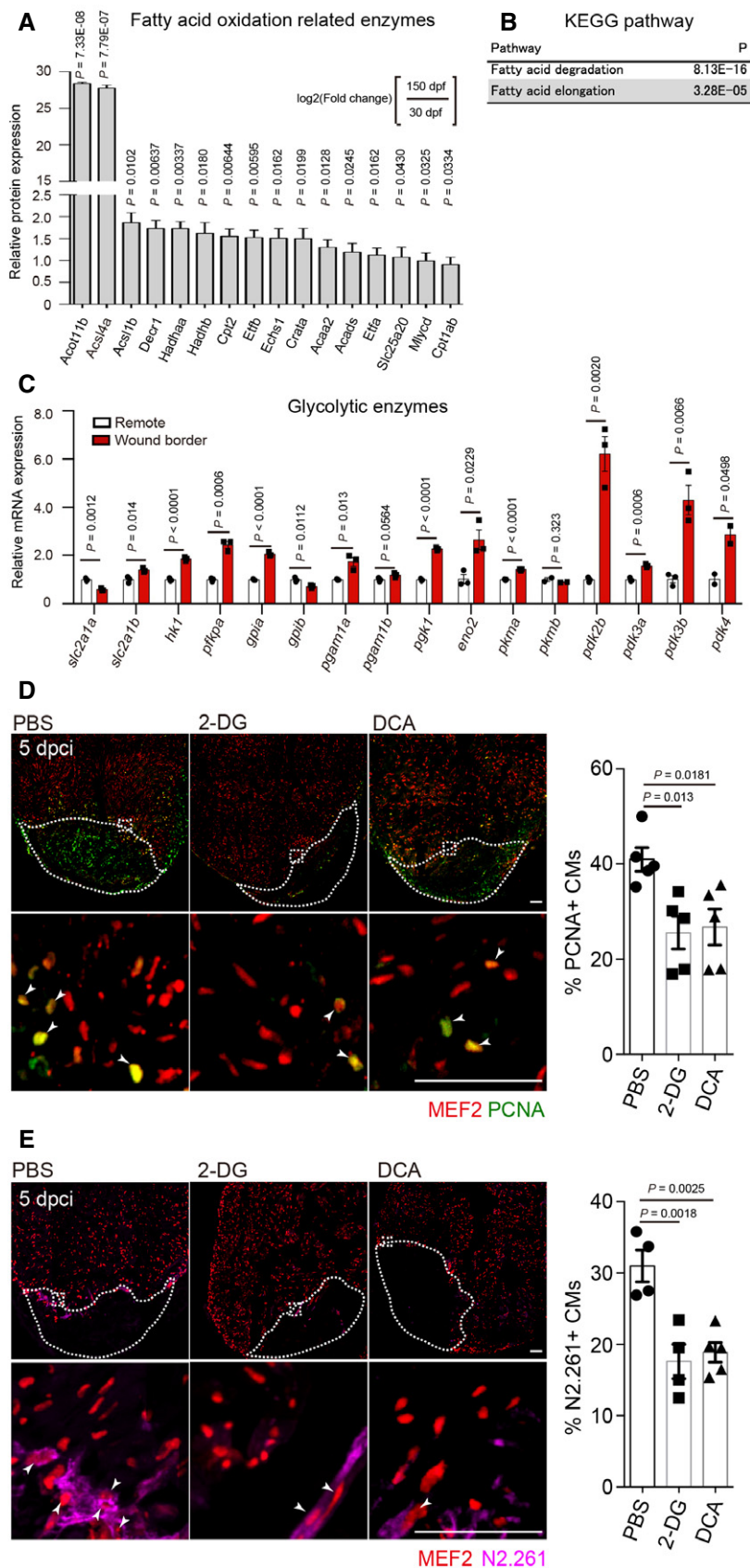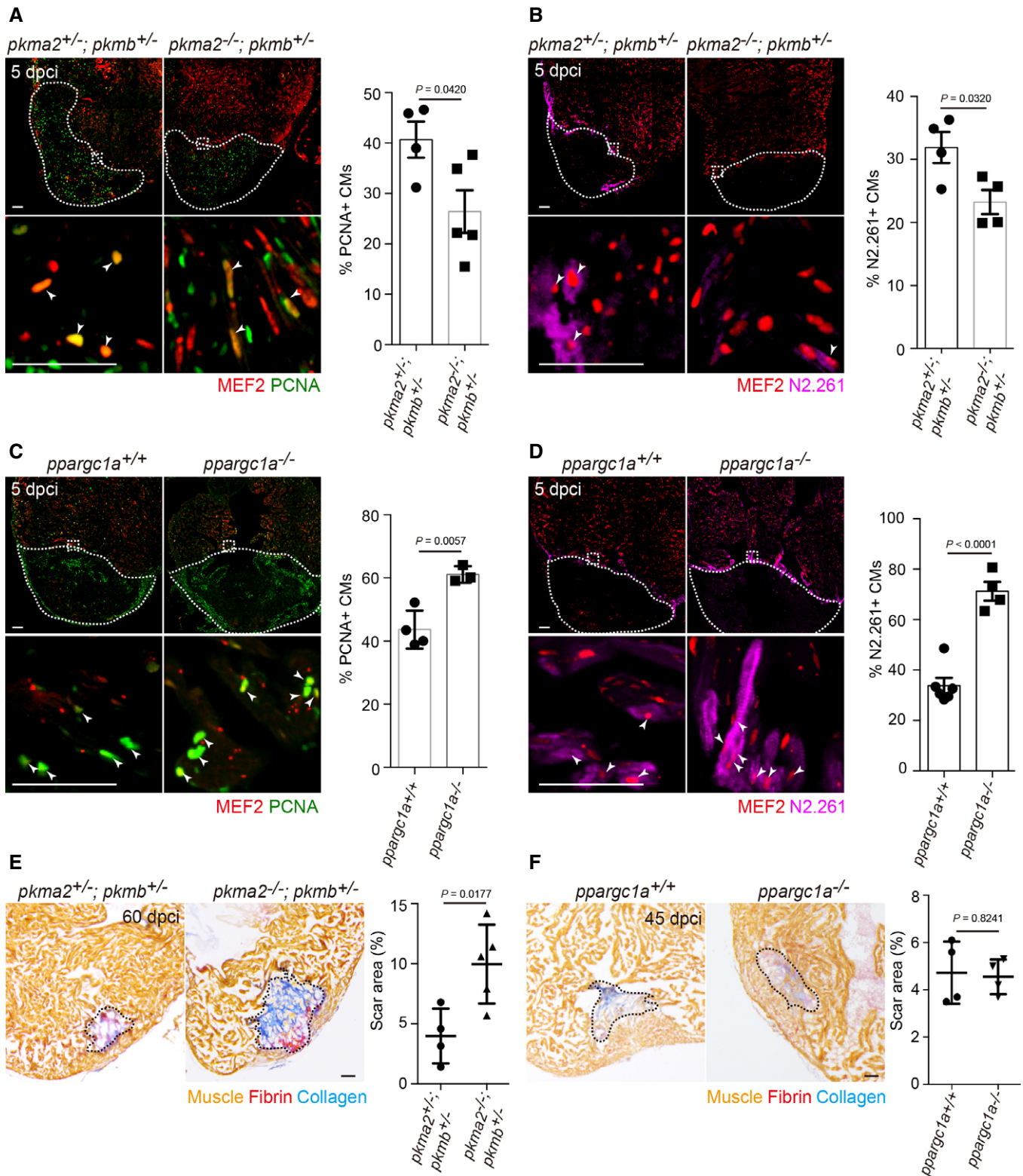
Figure 1.

Figure 2. Loss of *pkma2* and *ppargc1a* affects cardiomyocyte dedifferentiation and proliferation following cardiac injury.

A–D   Immunostaining of heart sections for PCNA and MEF2 (A, C) or N2.261 and MEF2 (B, D) in 5 dpci *pkma2*^+/−^; *pkmb*^+/−^ and *pkma2*^−/−^; *pkmb*^+/−^ (A, B) or *ppargc1a*^+/+^ and *ppargc1a*^−/−^ (C, D) animals; magnified view of area in white boxes shown below; arrowheads point to PCNA^+^ (A, C) or N2.261^+^ (B, D) CMs; white dashed lines outline the wound area; percentage of PCNA^+^ (A, C) or N2.261^+^ (B, D) CMs in the border zone shown on the right (*n* = 4–6 ventricles of each genotype).

E, F   AFOG staining of heart sections from 60 dpci *pkma2*^+/−^; *pkmb*^+/−^ and *pkma2*^−/−^; *pkmb*^+/−^ (E) or 45 dpci *ppargc1a*^+/+^ and *ppargc1a*^−/−^ (F) animals; black dashed lines outline the scar area; scar area measured on the right (*n* = 3–5 ventricles of each genotype).

Data information: Error bars, s.e.m.; *P* values were calculated by two-tailed unpaired *t*-test. Scale bars, 50 μm.

examined $pkma2^{-/-}$ animals and found that they exhibit a similar decrease in PCNA$^+$ and N2.261$^+$ CMs following cardiac injury (Figs EV2E and F). Together, these results suggest that reducing glycolysis by affecting Pkma2 function leads to an attenuation in CM dedifferentiation and proliferation during regeneration.

Conversely, in order to determine whether enhanced glycolytic activity can promote cardiac regeneration, we examined the role of *peroxisome proliferator-activated receptor gamma coactivator 1 alpha* (*ppargc1a*), which encodes a key regulator of mitochondrial oxidative metabolism (Lin *et al*, 2005). Forced *Ppargc1a* expression in CMs enhances oxygen consumption and mitochondrial respiration *in vitro* and *in vivo* (Lehman *et al*, 2000), while *Ppargc1a*-deficient mice exhibit decreased oxygen consumption in their left ventricular tissues (Lehman *et al*, 2008). Zebrafish *ppargc1a* mutant hearts exhibit reduced mitochondrial oxidative metabolism and increased glycolytic activity (Marin-Juez *et al*, 2019) without obvious cardiac defects (Fig EV2A–C). Altogether, these data suggest that in *ppargc1a* mutant hearts, pyruvate oxidation is reduced while metabolism of pyruvate to lactate is increased, and thus, *ppargc1a* mutants constitute a potential model of increased glycolysis. First, we examined the mRNA expression levels of *ppargc1a* and its targets *atp5pf* and *ndufb5* and found that these genes were downregulated in the cardiac tissues bordering the damaged area at 5 dpci (Fig EV2H). Notably, *ppargc1a* mutants exhibited an increase in proliferating CMs (Figs 2C and EV2G) as well as in the expression of embryonic myosin (Fig 2D) following cardiac injury, suggesting that promoting glycolysis in CMs can increase their dedifferentiation and proliferative potential. Furthermore, we examined $pkma2^{-/-}$; $pkmb^{+/-}$ animals at 60 dpci. We performed Acid Fuchsin Orange G (AFOG) staining to examine scar size. Notably, $pkma2^{-/-}$; $pkmb^{+/-}$ animals exhibited a significantly larger scar area compared to $pkma2^{+/-}$; $pkmb^{+/-}$ animals (Fig 2E). However, *ppargc1a* mutants did not exhibit a significant difference in scar area (Fig 2F). Together, these results provide further evidence that key regulators of pyruvate metabolism and glycolysis play an important role in CM dedifferentiation and proliferation in the early stages of cardiac regeneration.

Cardiomyocyte-specific modulation of pyruvate metabolism regulates cardiomyocyte behavior following cardiac injury

Expression analysis showed that multiple *pdk* genes were highly upregulated in tissues bordering the damaged area following cardiac injury (Fig 1C). Pdk promotes the conversion of pyruvate to lactate by inactivating the PDC through phosphorylation of pyruvate dehydrogenase E1 alpha 1 subunit (Pdha1), a catalytic subunit of the

PDC (Korotchkina & Patel, 2001; Rardin *et al*, 2009; Park *et al*, 2018). To impair glycolysis specifically in CMs, we used a form of Pdha1a (Pdha1aSTA), which cannot be phosphorylated by Pdk, leading to enhanced pyruvate conversion to acetyl-CoA (Hitosugi *et al*, 2011; Fan *et al*, 2014; Fukuda *et al*, 2019). Using the HOTcre system (Hesselson *et al*, 2009), we generated a *Tg(hsp70l:LOXP-STOP-LOXP-pdha1aSTA-T2A-mCherry)* line, which, when combined with the *Tg(myl7:Cre-ERT2)* line and following tamoxifen and heatshock treatments, expresses *pdha1aSTA* specifically in CMs to impair glycolysis (Fig EV3A). Consistent with our previous results with DCA treatments, which inhibit Pdk function, the number of proliferating CMs following cardiac injury was decreased in *Tg(myl7:Cre-ERT2); Tg(hsp70l:LOXP-STOP-LOXP-pdha1aSTA-T2A-mCherry)* animals after tamoxifen-induced recombination and heatshock treatments (Figs 3A and B, and EV3C). Conversely, in order to stimulate glycolysis in CMs, we generated a *Tg(hsp70l:LOX-STOP-LOXP-pdk3b-T2A-mCherry)* line and found that when *pdk3b* was overexpressed in *Tg(myl7:Cre-ERT2); Tg(hsp70l:LOXP-STOP-LOXP-pdk3b-T2A-mCherry)* animals (Fig EV3B), the number of proliferating CMs following cardiac injury was increased (Figs 3C and EV3D). We also examined the effects of *pdk3b* OE in noninjured hearts and saw no significant increase in the number of proliferating CMs (Fig EV3E). In line with their effects on CM proliferation, *pdha1aSTA* OE in CMs led to a decrease in the number of CMs exhibiting embryonic myosin expression, while *pdk3b* OE led to an increase (Fig 3D and E). Altogether, these results suggest that pyruvate metabolism as regulated by the PDK-PDC axis plays an important role in CM dedifferentiation and proliferation following cardiac injury. We next examined whether metabolic modulation in CMs affects scar size during cardiac regeneration, and found that *pdha1aSTA* OE led to the retention of a larger scar area at 60 dpci (Fig 3F), while *pdk3b* OE did not affect scar area (Fig 3G). Together with the data using metabolic enzyme mutant models, these results suggest that in the early stages of cardiac regeneration, glycolysis promotes CM dedifferentiation and proliferation and that genetic manipulations to enhance glycolytic activity do not facilitate scar resolution at later stages.

Modulation of pyruvate metabolism regulates primary rat neonatal cardiomyocyte cell cycle progression and behavior

We also tested the role of pyruvate metabolism in primary rat neonatal cardiomyocytes (RNCMs). To examine the role of pyruvate metabolism modulation in CM cell cycle progression, Ki67 expression was analyzed in RNCMs overexpressing PDHA1STA or PDK3 in growth culture medium containing 10% bovine serum as well as

Figure 3. Cardiomyocyte-specific modulation of pyruvate metabolism cell-autonomously affects their dedifferentiation and proliferation following cardiac injury.

A   Transgenic animals and experimental time course for data shown in (B–E).

B–E   Immunostaining of heart sections for PCNA and MEF2 (B, C) or N2.261 and MEF2 (D, E) in 5 dpci animals (*Tg(hsp70l:LOXP-STOP-LOXP-pdha1aSTA-T2A-mCherry)* and *Tg(hsp70l:LOXP-STOP-LOXP-pdk3b-T2A-mCherry)* alone (control) or in combination with *Tg(myl7:Cre-ERT2)*, all after tamoxifen and heat-shock treatments); magnified view of area in white boxes shown below; arrowheads point to PCNA$^+$ (B, C) or N2.261$^+$ (D, E) CMs; white dashed lines outline the wound area; percentage of PCNA$^+$ (B, C) or N2.261$^+$ (D, E) CMs in the border zone shown on the right (n = 4–5 ventricles of each genotype).

F, G   AFOG staining of heart sections from 60 dpci animals (*Tg(hsp70l:LOXP-STOP-LOXP-pdha1aSTA-T2A-mCherry)* (F) and *Tg(hsp70l:LOXP-STOP-LOXP-pdk3b-T2A-mCherry)* (G) alone (control) or in combination with *Tg(myl7:Cre-ERT2)*, all after tamoxifen and heat-shock treatments); black dashed lines outline the scar area; scar area measured on the right (n = 4–5 ventricles of each genotype).

Data information: Error bars, s.e.m.; P values were calculated by two-tailed unpaired t-test. Scale bars, 50 μm.
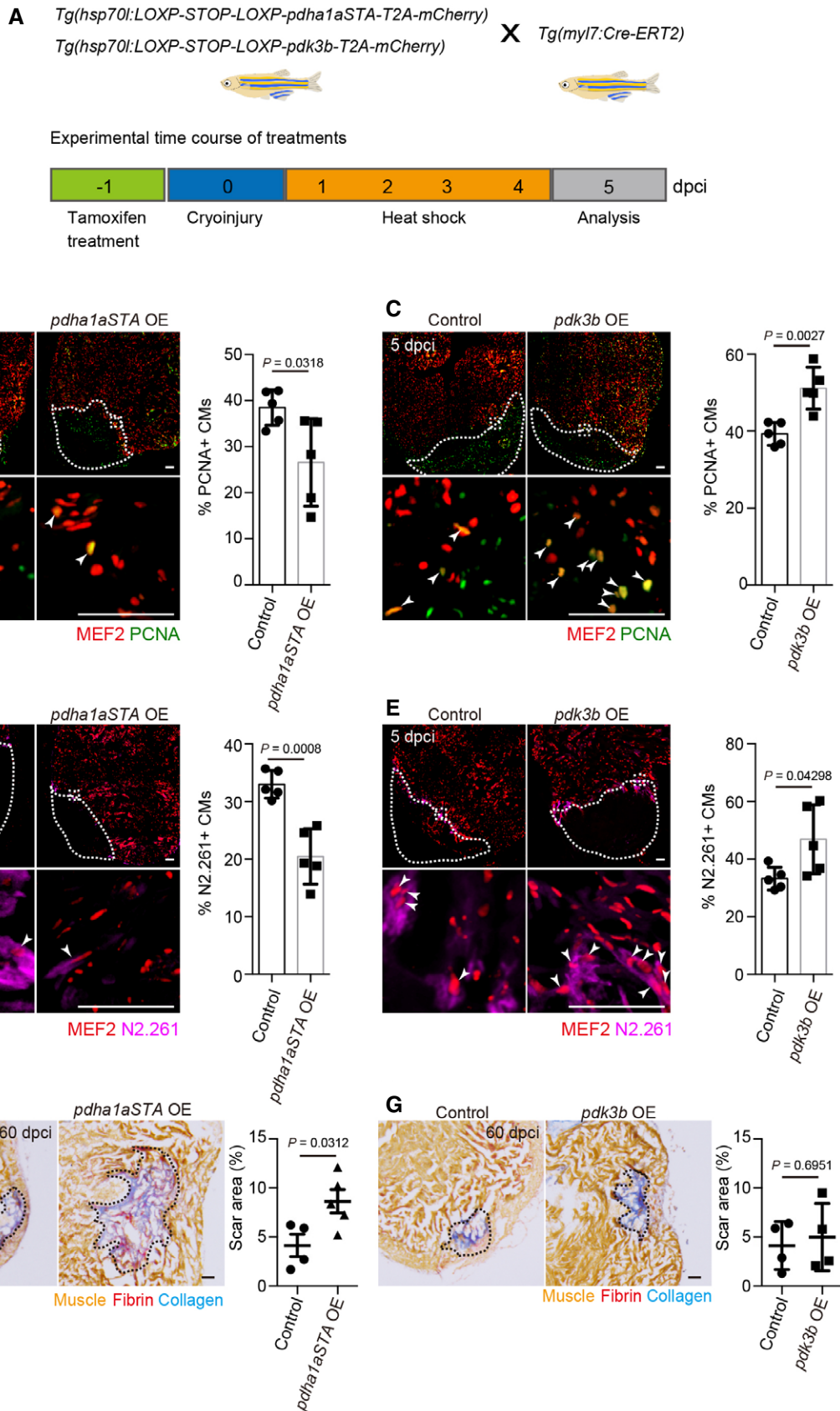
Figure 3.
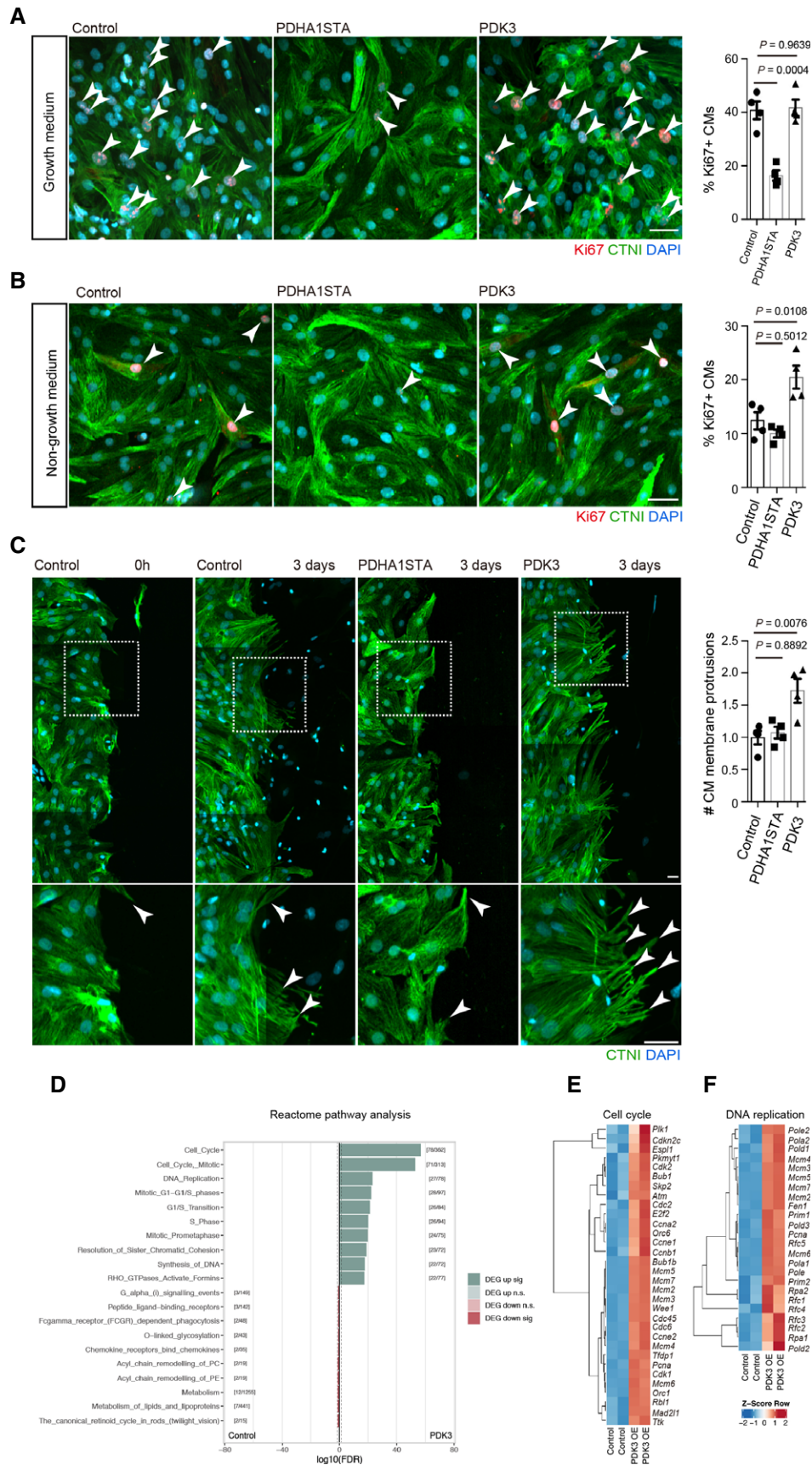
Figure 4.

Figure 4. Pyruvate metabolism modulation affects the behavior of rat neonatal cardiomyocytes in culture.

A, B   Staining for Ki67, CTNI, and DNA (DAPI) in control, PDHA1STA OE, or PDK3 OE RNCMs cultured in growth (A) or non-growth (B) medium; arrowheads point to Ki67^{+} RNCMs; percentage of Ki67^{+} RNCMs shown on the right (n = 4 biological replicates for each condition).

C   Staining for CTNI and DNA (DAPI) in scratch assay using control, PDHA1STA OE, or PDK3 OE RNCMs immediately or at 3 days after generating the scratch; magnified view of area in white boxes shown below; arrowheads point to membrane protrusions of RNCMs; quantification of CM membrane protrusions shown on the right (n = 4 biological replicates for each condition).

D   Reactome over-representation analysis of differentially regulated genes in PDK3 OE RNCMs compared to control.

E, F   Heat map of gene expression for key regulators of cell cycle (E) and DNA replication (F) in PDK3 OE vs. control RNCMs.

Data information: Error bars, s.e.m.; P values were calculated by ordinary one-way ANOVA with Dunnett's multiple comparison test (A–C) or Benjamini–Hochberg correction (D). Scale bars, 20 μm.

in non-growth culture medium. We found that PDHA1STA OE significantly decreased the number of Ki67^{+} RNCMs in growth conditions (Fig 4A), while PDK3 OE increased the number of Ki67^{+} RNCMs (Fig 4B) in non-growth conditions. PDK3 OE also led to an increase in the number of pHH3[+] RNCMs (Fig EV4C). We then determined cell numbers and found that PDHA1STA OE significantly decreased the number of RNCMs (Fig EV4D), while PDK3 OE did not lead to obvious changes (Fig EV4E). Next, we investigated the role of pyruvate metabolism in an *in vitro* scratch assay which is used to examine the ability of cells to fill a wound-like gap in a confluent cell monolayer (Cormier *et al*, 2015). We first examined CM cell cycle progression in the scratch assay and found no significant differences in the number of Ki67^{+} CMs in the area close to the scratch border compared to the remote area (Fig EV4A and B). We then examined CM behavior and found that RNCMs close to the scratch border exhibited membrane protrusions (Fig 4C). Similar observations have been reported when analyzing zebrafish and mouse regeneration models, where CMs replenish to the injured area (Itou *et al*, 2012; Morikawa *et al*, 2015; Tahara *et al*, 2016; Marin-Juez *et al*, 2019; preprint: Aharonov *et al*, 2020). We analyzed the effects of pyruvate metabolism modulation on CM behavior in the scratch assay and found that PDK3 OE led to an increase in the number of CM membrane protrusions (Figs 4C and EV4C). To gain insight into the signaling pathways and effectors that are regulated by PDK3 OE in RNCMs, we performed transcriptomic analysis. Notably, the resulting data indicate that PDK3 OE led to increased levels of genes encoding factors which promote DNA replication and cell cycle (Figs 4D–F and EV4F and G). Altogether, these data indicate that pyruvate metabolism regulated by PDK also promotes mammalian CM cell cycle progression and protrusive behavior.

Glycolysis plays an important role in the proliferation of cancer cells (Liberti & Locasale, 2016), endothelial cells (De Bock *et al*, 2013; Wilhelm *et al*, 2016), and neural progenitor cells (Zheng *et al*, 2016), as well as during cardiac (Wang *et al*, 2018; Honkoop *et al*, 2019; Magadum *et al*, 2020) and skeletal muscle (Wagner *et al*, 1976; Magadum & Engel, 2018) regeneration. Here, we showed that CM-specific modulation of glycolysis also regulates CM dedifferentiation and proliferation during regeneration. In addition, our transcriptomic data show that PDK3 OE, which enhances glycolysis, leads to higher levels of cell cycle regulator gene expression in RNCMs. It will of course be important to investigate further how glycolysis regulates these processes.

Our data indicate that increased glycolysis by Pdk3 OE promotes CM dedifferentiation following cardiac injury. It was reported that in regenerating CMs, mitochondria exhibit an immature structure and that the levels of mitochondrial gene expression

are reduced (Honkoop *et al*, 2019), indicating lower mitochondrial activity. In addition, mitochondrial function increases during CM maturation in the developing heart (Menendez-Montes *et al*, 2016). Thus, reduced mitochondrial activity, and thereby reduced OXPHOS, may be important for CM dedifferentiation and proliferation during regeneration.

It has also been shown that the levels of glycolytic enzymes increase following cardiac ischemia and in failing hearts (Das *et al*, 1987; Doenst *et al*, 2013). However, adult mice do not exhibit robust cardiac regeneration. Recent data show that the upregulation of PKM2 levels following cardiac injury is limited and thus possibly insufficient to promote CM proliferation in an ischemic adult mouse model (Magadum *et al*, 2020), while *Pkm2* OE induced CM proliferation after cardiac injury (Magadum *et al*, 2020). Together, these data suggest that the levels of glycolytic gene expression in mice following cardiac injury might be a limiting factor in terms of promoting CM proliferation. It will be interesting to further investigate the differences in metabolic changes between zebrafish and mouse cardiac injury models.

During cardiac regeneration, it is assumed that newly divided CMs have to undergo maturation to generate fully functional cardiac tissue. During development, the metabolic shift from glycolysis to OXPHOS plays an important role in CM differentiation and maturation (Cho *et al*, 2006; Chung *et al*, 2007). Our data in zebrafish indicate that while enhanced glycolysis by Pdk3 OE promotes CM proliferation during the early stages of cardiac regeneration, scar resolution at later stages does not appear to be significantly affected. However, it remains unclear whether, in conditions of Pdk3 OE, the newly formed CMs have undergone maturation and also whether CM maturation promotes scar resolution. Clearly, many questions remain to be addressed to fully understand the role of metabolism during cardiac regeneration.

Together, our data indicate that cardiac metabolism regulated by the PDK-PDC axis promotes CM proliferation following cardiac injury in zebrafish as well as cell cycle progression of mammalian CMs in culture.

Materials and Methods

Zebrafish

All zebrafish husbandry was performed under standard conditions in accordance with FELASA guidelines (Aleström *et al*, 2019) and institutional (MPG) and national ethical and animal welfare guidelines. The following transgenic lines and mutants were used: *Tg(cryaa:DsRed,-5.1myl7:CreERT2)[pd10]* (Kikuchi *et al*,

2010) abbreviated *Tg(myl7:CreERT2)*, *pkma2^s717^* (Stone *et al*, 2018), *pkmb^s718^* (Stone *et al*, 2018), and *ppargc1a^bns176^* (Marin-Juez *et al*, 2019). To generate *Tg(cryaa:Cerulean,hsp70l:LOXP-STOP-LOXP-pdha1aSTA-T2A-mCherry)^bns343^* abbreviated *Tg(hsp70l:LOXP-STOP-LOXP-pdha1aSTA-T2A-mCherry)* and *Tg(cryaa:Cerulean,hsp70l:LOXP-STOP-LOXP-pdk3b-T2A-mCherry)^bns344^* abbreviated *Tg(hsp70l:LOXP-STOP-LOXP-pdk3b-T2A-mCherry)*, *pdk3b* (NM_001080688) and *pdha1a* (NM_213393) were isolated by RT–PCR and cloned into a vector containing a promoter of *heat-shock cognate 70-kd protein, like* (*hsp70l*), and two I-SceI restriction sites. The following primers were used to amplify the cDNA: *pdk3b* (forward 5′-TTCCACTAGTGCTCCACCGGTCCACCATGAAAC TGTTTATCTG-3′ and reverse 5′-GCCCTCTCCACTGCCCTCGAGT CTGTTGACTTTGTATGTGGA-3′); *pdha1a* (forward 5′-TTCCAC TAGTGCTCCACCGGTCCACCATGAGAAAGATGC-3′ and reverse 5′-GCCCTCTCCACTGCCCTCGAGGCTGATGGACTTGAGTTTG-3′). Plasmids were then injected into one-cell-stage embryos with I-SceI (NEB).

Cryoinjury and quantification

Cryoinjury was performed as previously described (González-Rosa *et al*, 2011). Confocal images were processed using the ZEN software (ZEISS), and PCNA$^+$, N2.261$^+$, or pHH3$^+$ CMs in the 50-μm region adjacent to the injured area at 5 dpci were counted. The percentage of PCNA$^+$, N2.261$^+$, or pHH3$^+$ CMs in the border zone was calculated by dividing the number of PCNA$^+$, N2.261$^+$, or pHH3$^+$ CMs by the total number of CMs.

Pharmacological treatments

Adult zebrafish were treated with PBS, 2-DG (1 nmol/mg body weight; Sigma-Aldrich), or DCA (0.5 nmol/mg body weight; Sigma-Aldrich) by intraperitoneal (IP) injections (Kinkel *et al*, 2010) from 1 to 4 dpci and analyzed at 5 dpci.

Tamoxifen and heat-shock treatments

To induce Cre-ERT2-mediated recombination, animals were treated with 10 μM 4-hydroxytamoxifen (4-HT; Sigma-Aldrich) by IP injection. Cryoinjury was performed 24 h after 4-HT injection. Heat-shock treatments were performed in a 37°C water bath for 1 h per day from 1 to 4 dpci, and animals were analyzed at 5 dpci. To examine 60 dpci hearts in transgenic animals (Fig 3F and G), heat-shock treatments were performed five to seven times a week from 1 to 59 dpci.

Staining

Zebrafish heart sections and RNCMs were fixed in 4% paraformaldehyde. Anti-MEF2 1:50 (sc-313, Santa Cruz Biotechnology), anti-PCNA 1:500 (PC10, Santa Cruz Biotechnology), anti-N2.261 1:100 (N2.261, DSHB), anti-DsRed 1:500 (632496, Takara), anti-MHC 1:500 (MF20, DSHB), anti-phospho-histone H3 1:200 (06-570, EMD Millipore), and anti-cardiac troponin I (CTNI) 1:500 (ab56357, Abcam) were used. After washing with PBS, samples were stained with Alexa 568, Alexa 488, or Alexa 647 secondary antibodies 1:500 (Life Technologies), followed by

4′,6-diamidine-2′-phenylindole dihydrochloride (DAPI) 1:2,000 (Merck) staining to visualize DNA. To count PCNA$^+$, N2.261$^+$, or pHH3$^+$ CMs in regenerating ventricles, we analyzed more than three sections from each heart. Acid Fuchsin Orange G (AFOG) staining was performed using the A.F.O.G. Kit (BIOGNOST).

Cell culture

Rat neonatal (P1–P3) CMs were isolated as previously described (Fukuda *et al*, 2017), and CMs were further separated by density gradient centrifugation (Golden *et al*, 2012). Cells were plated onto 0.1% gelatin-coated (Sigma) plates and cultured in DMEM/F12 (Gibco) supplemented with 5% horse serum, L-glutamine, Na pyruvate, penicillin, and streptomycin at 37°C and 5% CO$_2$. 10% FBS (HyClone) was added to the medium for the growth conditions. CMs were transfected with adenovirus vectors and cultured for 72 h in growth medium or non-growth medium. Samples were then fixed with 4% PFA and stained with anti-CTNI and DAPI. Five different 1,000 μm regions per sample were analyzed for CM numbers, and average values were used.

Lactate measurements

Lactate levels were measured using a PicoProbe Lactate Fluorometric Assay Kit (BioVision). For each condition, the cryoinjured area and adjacent tissue from 10 ventricles were collected in PBS and homogenized. Samples were centrifuged, and the supernatant was used to measure lactate levels according to manufacturer's protocol. Fluorescence was detected with a FLUOstar Omega instrument (BMG).

Adenovirus vectors

Adenovirus vectors for transfection into CMs were generated using the AdEasy system (Agilent Technologies). The adenovirus vector encoding *Pdk3* was previously described (Fukuda *et al*, 2019). To amplify *Pdha1* (NM_008810) from mouse tissues, the following primers were used: *Pdha1* (forward 5′-TAGAGATCTGGTACCGTC GACcACCATGAGGAAGATGCTTGCC-3′ and reverse 5′-GGATATCT TATCTAGAAGCTTAACTGACTGACTTAAACTTGATC). To generate *Pdha1STA*, the following primers were used: forward 5′-TACCGC TACCATGGACACGCCATGAGTGACCCTGGAGTAAGCGCCCGCACTC GAGAAGAAATC-3′ and reverse 5′-GATTTCTTCTCGAGTGCGGGCGC TTACTCCAGGGTCACTCATGGCGTGTCCATGGTAGCGGTA-3′

Scratch assay

CMs were cultured in growth medium until the plates were confluent and then transfected with adenovirus vectors encoding the gene of interest. After 24 h of culture, a sterilized plastic ruler was laid on the plate, and a sterile pipette tip was used to make a scratch in the CM layer as previously described (Cormier *et al*, 2015). After removing the dead cells, the plates were incubated for 3 days and then analyzed. To quantify CM membrane protrusions in the scratch assay, the number of CM membrane protrusions in an area of 1,000 μm height × 200 μm width was determined. The average value from two different regions per

sample was used. Values were normalized to the average value of control.

Imaging

A Zeiss spinning disk confocal microscope (CSU-X1, Yokogawa) and ORCA-Flash4.0 sCMOS camera (Hamamatsu) were used to acquire images. Time-lapse imaging for the scratch assay was performed using an SP8 microscope (Leica).

RT–qPCR

The miRNeasy Mini Kit (Qiagen) was used for total RNA extraction, and cDNA was synthesized using the SuperScript Second Strand Kit (Life Technologies). The CFX Connect Real-Time System (Bio-Rad) and DyNAmo ColorFlash SYBR Green qPCR Kit (Thermo Fisher Scientific) were used. Technical replicates were analyzed for each sample. Primer sequences are shown in Table EV1 and Ct values in Table EV2.

Statistical analysis

Benjamini–Hochberg-corrected P values as well as standard errors for the fold changes represented by error bars were calculated using limma for proteomic analysis (Fig 1A and B). Comparative statistics between two sample groups was performed using two-tailed unpaired t-test and between more than two sample groups using ordinary one-way ANOVA with Dunnett's multiple comparison test for parametric data. Benjamini–Hochberg correction was used for RNA-seq data analysis.

Mass spectrometry

Zebrafish ventricles were homogenized with a grinder in SDS lysis buffer (4% SDS in 0.1 M Tris–HCl pH 7.6) and heated at 70°C for 10 min. For DNA shearing, samples were sonicated prior to sedimentation of cell debris by centrifugation at 16,000 g for 10 min. Cleared supernatants were subjected to estimation of protein concentration (DC protein assay, Bio-Rad). Protein samples were separated according to their molecular weight by SDS–PAGE (NuPAGE 4–12% Bis-Tris Gel, Thermo Scientific), stained by InstantBlue Coomassie staining (Expedeon), and subjected to in-gel digestion (Shevchenko *et al*, 2006). Finally, samples were desalted and stored on STop And Go Extraction (STAGE) tips (Rappsilber *et al*, 2003) prior to analysis by liquid chromatography–tandem mass spectrometry (LC-MS/MS). Capillary LC was performed in line to a Q Exactive HF mass spectrometer (Thermo Scientific) via an electrospray ionization (ESI) source using a nano-UHPLC System (EASY-nLC 1000, Thermo Scientific), as well as an in-house packed 70 μm ID, 15-cm reverse-phase column emitter (ReproSil-Pur 120 C18-AQ, 1.9 μm, Dr. Maisch GmbH) with a buffer system comprising solvent A (5% acetonitrile and 1% formic acid) and solvent B (80% acetonitrile and 1% formic acid). Relevant instrumentation parameters were extracted using MARMoSET (Kiweler *et al*, 2019) and are included in the Appendix information. Raw data processing was done using the MaxQuant suite of algorithms (v. 1.6.8.0) (Cox & Mann, 2008)

against the *Danio rerio* UniProtKB database (canonical and isoforms; downloaded on 2019/08/19; 62,099 entries) with parameters documented in the supplementary material and employing label-free quantitation (Cox *et al*, 2014). Downstream bioinformatics analysis was performed using a limma-based R pipeline (Ritchie *et al*, 2015) (https://github.com/bhagwatadity/autonomics), on logarithmized intensities provided by MaxQuant and including an over-representation analysis by Fisher's exact test, testing for enrichment of KEGG annotation terms in protein groups significantly ($P \leq 0.05$) upregulated in 150 dpf vs. 30 dpf hearts as compared to the detectome, the total of all detected protein groups.

RNA-seq analysis

Total RNA was isolated from RNCMs using the miRNeasy Mini Kit (Qiagen). RNA and library preparation integrity were verified with LabChip GX Touch 24 (Perkin Elmer). 1 μg of total RNA was used as input for VAHTS Stranded mRNA-seq Library Preparation following manufacturer's protocol (Vazyme). Sequencing was performed on a NextSeq 500 instrument (Illumina) using v2 chemistry, resulting in an average of 37 M reads per library with 1×75 bp single-end setup. The resulting raw reads were assessed for quality, adapter content, and duplication rates with FastQC (http://www.bioinformatics.babraham.ac.uk/projects/fastqc). Trimmomatic version 0.39 was employed to trim reads after a quality drop below a mean of Q20 in a window of 5 nucleotides (Bolger *et al*, 2014). Only reads between 30 and 150 nucleotides were cleared for further analyses. Trimmed and filtered reads were aligned vs. the Ensembl Rat genome version rn6 (version 94) using STAR 2.6.1d with the parameter "–outFilterMismatchNoverLmax 0.1" to increase the maximum ratio of mismatches to mapped length to 10% (STAR: ultrafast universal RNA-seq aligner) (Dobin *et al*, 2013). The number of reads aligning to genes was counted with featureCounts 1.6.5 tool from the Subread package (Liao *et al*, 2014). Only reads mapping at least partially inside exons were admitted and aggregated per gene. Reads overlapping multiple genes or aligning to multiple regions were excluded. Differentially expressed genes were identified using DESeq2 version 1.26.0 (Love *et al*, 2014). Only genes with a minimum fold change of ± 2 ($\log_2 = \pm 1$), a maximum Benjamini–Hochberg-corrected P-value of 0.05, and a minimum combined mean of 5 reads were deemed to be significantly differentially expressed. The Ensembl annotation was enriched with UniProt data (release 17.12.2018) based on Ensembl gene identifiers (Activities at the Universal Protein Resource (UniProt)). Gene Ontology analyses were performed using KEGG (https://www.genome.jp/kegg/kegg_ja.html), Reactome (https://reactome.org/), and KOBAS 2.0 (Xie *et al*, 2011). Two separate tests were performed per contrast using only either up- or down-regulated genes for analysis. The results were combined keeping only gene sets that showed significant over-representation at FDR < 0.2 in only one input list (i.e., that were clearly enriched for up- or down-regulated genes, but not both). The Top10 gene sets considering enrichment FDR were selected per direction of regulation. The dashed line represents an FDR of 0.05, while the values in brackets denote the number of regulated genes vs. total genes in the respective pathway (Figs 4D and EV4F and G).

Data availability

Expanded View for this article is available online.

Author contributions

RF designed and conducted most experiments; RF and DYRS analyzed the data and wrote the paper; RM-J and HES designed and performed the experiments; AB and RM-J helped with the writing; RR helped with live imaging; CK and SG conducted transcriptome analysis; and AK, AMB, and JG conducted proteome analysis. All authors commented on the manuscript.

Conflict of interest

The authors declare no competing financial interests.

References

Aharonov A, Shakked A, Umansky KB, Savidor A, Kain D, Lendengolts D, Revach O-Y, Morikawa Y, Dong J, Levin Y *et al* (2020) ERBB2 drives YAP activation and EMT-like processes during cardiac regeneration. *BioRxiv* https://doi.org/10.1101/2020.01.07.897199 [PREPRINT]

Aleström P, D'Angelo L, Midtlyng PJ, Schorderet DF, Schulte-Merker S, Sohm F, Warner S (2019) Zebrafish: housing and husbandry recommendations. *Lab Anim* https://doi.org/10.1177/0023677219869037

Behal RH, Buxton DB, Robertson JG, Olson MS (1993) Regulation of the pyruvate dehydrogenase multienzyme complex. *Annu Rev Nutr* 13: 497−529

Beisaw A, Kuenne C, Guenther S, Dallman J, Wu CC, Bentsen M, Looso M, Stainier DYR (2020) AP-1 contributes to chromatin accessibility to promote sarcomere disassembly and cardiomyocyte protrusion during zebrafish heart regeneration. *Circ Res* https://doi.org/10.1161/CIRCRESAHA.119.316167

Ben-Yair R, Butty VL, Busby M, Qiu Y, Levine SS, Goren A, Boyer LA, Burns CG, Burns CE (2019) H3K27me3-mediated silencing of structural genes is required for zebrafish heart regeneration. *Development* 146: dev178632

Bolger AM, Lohse M, Usadel B (2014) Trimmomatic: a flexible trimmer for Illumina sequence data. *Bioinformatics* 30: 2114−2120

Cho YM, Kwon S, Pak YK, Seol HW, Choi YM, Park DJ, Park KS, Lee HK (2006) Dynamic changes in mitochondrial biogenesis and antioxidant enzymes during the spontaneous differentiation of human embryonic stem cells. *Biochem Biophys Res Commun* 348: 1472−1478

Christofk HR, Vander Heiden MG, Harris MH, Ramanathan A, Gerszten RE, Wei R, Fleming MD, Schreiber SL, Cantley LC (2008) The M2 splice isoform of pyruvate kinase is important for cancer metabolism and tumour growth. *Nature* 452: 230−233

Chung S, Dzeja PP, Faustino RS, Perez-Terzic C, Behfar A, Terzic A (2007) Mitochondrial oxidative metabolism is required for the cardiac differentiation of stem cells. *Nat Clin Pract Cardiovasc Med* 4: S60−S67

Chung S, Arrell DK, Faustino RS, Terzic A, Dzeja PP (2010) Glycolytic network restructuring integral to the energetics of embryonic stem cell cardiac differentiation. *J Mol Cell Cardiol* 48: 725−734

Cormier N, Yeo A, Fiorentino E, Paxson J (2015) Optimization of the wound scratch assay to detect changes in murine mesenchymal stromal cell migration after damage by soluble cigarette smoke extract. *J Vis Exp* 2015: 1−9

Cox J, Mann M (2008) MaxQuant enables high peptide identification rates, individualized p.p.b.-range mass accuracies and proteome-wide protein quantification. *Nat Biotechnol* 26: 1367−1372

Cox J, Hein MY, Luber CA, Paron I, Nagaraj N, Mann M (2014) Accurate proteome-wide label-free quantification by delayed normalization and maximal peptide ratio extraction, termed MaxLFQ. *Mol Cell Proteomics* 13: 2513−2526

Das DK, Engelman RM, Rousou JA, Breyer RH (1987) Aerobic vs anaerobic metabolism during ischemia in heart muscle. *Ann Chir Gynaecol* 76: 68−76

De Bock K, Georgiadou M, Schoors S, Kuchnio A, Wong BW, Cantelmo AR, Quaegebeur A, Ghesquière B, Cauwenberghs S, Eelen G *et al* (2013) Role of PFKFB3-driven glycolysis in vessel sprouting. *Cell* 154: 651−663

Dobin A, Davis CA, Schlesinger F, Drenkow J, Zaleski C, Jha S, Batut P, Chaisson M, Gingeras TR (2013) STAR: ultrafast universal RNA-seq aligner. *Bioinformatics* 29: 15−21

Doenst T, Nguyen TD, Abel ED (2013) Cardiac metabolism in heart failure: implications beyond ATP production. *Circ Res* 113: 709−724

Fan J, Kang HB, Shan C, Elf S, Lin R, Xie J, Gu TL, Aguiar M, Lonning S, Chung TW *et al* (2014) Tyr-301 phosphorylation inhibits pyruvate dehydrogenase by blocking substrate binding and promotes the Warburg effect. *J Biol Chem* 289: 26533−26541

Fukuda R, Gunawan F, Beisaw A, Jimenez-Amilburu V, Maischein HM, Kostin S, Kawakami K, Stainier DYR (2017) Proteolysis regulates cardiomyocyte maturation and tissue integration. *Nat Commun* 8: 14495

Fukuda R, Aharonov A, Ong YT, Stone OA, El-Brolosy M, Maischein HM, Potente M, Tzahor E, Stainier DYR (2019) Metabolic modulation regulates cardiac wall morphogenesis in zebrafish. *eLife* 8: e50161

Fukushima A, Alrob OA, Zhang L, Wagg CS, Altamimi T, Rawat S, Rebeyka IM, Kantor PF, Lopaschuk GD (2019) Acetylation and succinylation contribute to maturational alterations in energy metabolism in the newborn heart. *Am J Physiol Heart Circ Physiol* 311: H347–H363

Golden HB, Gollapudi D, Gerilechaogetu F, Li J, Cristales RJ, Peng X, Dostal DE (2012) Isolation of cardiac myocytes and fibroblasts from neonatal rat pups. *Methods Mol Biol* 843: 205−214

González-Rosa JM, Martin V, Peralta M, Torres M, Mercader N (2011) Extensive scar formation and regression during heart regeneration after cryoinjury in zebrafish. *Development* 138: 1663−1674

Grajevskaja V, Camerota D, Bellipanni G, Balciuniene J, Balciunas D (2018) Analysis of a conditional gene trap reveals that tbx5a is required for heart regeneration in zebrafish. *PLoS ONE* 13: 1−14

Gudi R, Bowker-Kinley MM, Kedishvili NY, Zhao Y, Popov KM (1995) Diversity of the pyruvate dehydrogenase kinase gene family in humans. *J Biol Chem* 270: 28989−28994

Hesselson D, Anderson RM, Beinat M, Stainier DYR (2009) Distinct populations of quiescent and proliferative pancreatic β-cells identified by HOTcre mediated labeling. *Proc Natl Acad Sci USA* 106: 14896−14901

Hitosugi T, Fan J, Chung TW, Lythgoe K, Wang X, Xie J, Ge Q, Gu TL, Polakiewicz RD, Roesel JL et al (2011) Tyrosine phosphorylation of mitochondrial pyruvate dehydrogenase kinase 1 is important for cancer metabolism. Mol Cell 44: 864–877

Honkoop H, de Bakker DE, Aharonov A, Kruse F, Shakked A, Nguyen PD, de Heus C, Garric L, Muraro MJ, Shoffner A et al (2019) Single-cell analysis uncovers that metabolic reprogramming by ErbB2 signaling is essential for cardiomyocyte proliferation in the regenerating heart. eLife 8: e50163

Itou J, Oishi I, Kawakami H, Glass TJ, Richter J, Johnson A, Lund TC, Kawakami Y (2012) Migration of cardiomyocytes is essential for heart regeneration in zebrafish. Development 139: 4133–4142

Jopling C, Sleep E, Raya M, Marti M, Raya A, Izpisua Belmonte JC (2010) Zebrafish heart regeneration occurs by cardiomyocyte dedifferentiation and proliferation. Nature 464: 606–609

Kikuchi K, Holdway JE, Werdich AA, Anderson RM, Fang Y, Egnaczyk GF, Evans T, Macrae CA, Stainier DYR, Poss KD (2010) Primary contribution to zebrafish heart regeneration by gata4(+) cardiomyocytes. Nature 464: 601–605

Kim Y, Lee YS, Kang SW, Kim S, Kim TY, Lee SH, Hwang SW, Kim J, Kim EN, Ju JS et al (2019) Loss of PKM2 in Lgr5^{+} intestinal stem cells promotes colitis-associated colorectal cancer. Sci Rep 9: 6212

Kinkel MD, Eames SC, Philipson LH, Prince VE (2010) Intraperitoneal injection into adult zebrafish. J Vis Exp 42: 2126

Kiweler M, Looso M, Graumann J (2019) MARMoSET — extracting publication-ready mass spectrometry metadata from RAW files. Mol Cell Proteomics 18: 1700–1702

Kolwicz SC Jr, Purohit S, Tian R (2013) Cardiac metabolism and its interactions with contraction, growth, and survival of cardiomyocytes. Circ Res 113: 603–616

Korotchkina LG, Patel MS (2001) Site specificity of four pyruvate dehydrogenase kinase isoenzymes toward the three phosphorylation sites of human pyruvate dehydrogenase. J Biol Chem 276: 37223–37229

Koukourakis MI, Giatromanolaki A, Sivridis E, Gatter KC, Harris AL (2005) Pyruvate dehydrogenase and pyruvate dehydrogenase kinase expression in non small cell lung cancer and tumor-associated stroma. Neoplasia 7: 1–6

Kreipke R, Wang Y, Miklas JW, Mathieu J, Ruohola-Baker H (2016) Metabolic remodeling in early development and cardiomyocyte maturation. Semin Cell Dev Biol 52: 84–92

Leclerc D, Pham DN, Levesque N, Truongcao M, Foulkes WD, Sapienza C, Rozen R (2017) Oncogenic role of PDK4 in human colon cancer cells. Br J Cancer 116: 930–936

Lehman JJ, Barger PM, Kovacs A, Saffitz JE, Medeiros DM, Kelly DP (2000) Peroxisome proliferator-activated receptor gamma coactivator-1 promotes cardiac mitochondrial biogenesis. J Clin Invest 106: 847–856

Lehman JJ, Boudina S, Banke NH, Sambandam N, Han X, Young DM, Leone TC, Gross RW, Lewandowski ED, Abel ED et al (2008) The transcriptional coactivator PGC-1alpha is essential for maximal and efficient cardiac mitochondrial fatty acid oxidation and lipid homeostasis. Am J Physiol Heart Circ Physiol 295: H185–H196

Lehninger AL, Nelson DL, Cox MM (2005) Principles of biochemistry, 4th edn. New York, NY: Worth

Liao Y, Smyth GK, Shi W (2014) featureCounts: an efficient general purpose program for assigning sequence reads to genomic features. Bioinformatics 30: 923–930

Liberti MV, Locasale JW (2016) The Warburg effect: how does it benefit cancer cells? Trends Biochem Sci 41: 211–218

Lin J, Handschin C, Spiegelman BM (2005) Metabolic control through the PGC-1 family of transcription coactivators. Cell Metab 1: 361–370

Love MI, Huber W, Anders S (2014) Moderated estimation of fold change and dispersion for RNA-seq data with DESeq2. Genome Biol 15: 550

Lunt SY, Muralidhar V, Hosios AM, Israelsen WJ, Gui DY, Newhouse L, Ogrodzinski M, Hecht V, Xu K, Acevedo PNM et al (2015) Pyruvate kinase isoform expression alters nucleotide synthesis to impact cell proliferation. Mol Cell 57: 95–107

Magadum A, Engel FB (2018) PPARβ/δ: linking metabolism to regeneration. Int J Mol Sci 19: 2013

Magadum A, Singh N, Kurian AA, Munir I, Mehmood T, Brown K, Sharkar M, Chepurko E, Sassi Y, Oh JG et al (2020) Pkm2 regulates cardiomyocyte cell cycle and promotes cardiac regeneration. Circulation 141: 1249–1265

Marin-Juez R, El-Sammak H, Helker CSM, Kamezaki A, Mullapuli ST, Bibli S-I, Foglia MJ, Fleming I, Poss KD, Stainier DYR (2019) Coronary revascularization is regulated by epicardial and endocardial cues and forms a scaffold for cardiomyocyte repopulation. Dev Cell 51: 503–515

Menendez-Montes I, Escobar B, Palacios B, Gómez MJ, Izquierdo-Garcia JL, Flores L, Jiménez-Borreguero LJ, Aragones J, Ruiz-Cabello J, Torres M et al (2016) Myocardial VHL-HIF signaling controls an embryonic metabolic switch essential for cardiac maturation. Dev Cell 39: 724–739

Morikawa Y, Zhang M, Heallen T, Leach J, Tao G, Xiao Y, Bai Y, Li W, Willerson JT, Martin JF (2015) Actin cytoskeletal remodeling with protrusion formation is essential for heart regeneration in Hippo-deficient mice. Sci Signal 8: ra41

Neely JR, Morgan HE (1974) Relationship between carbohydrate and lipid metabolism and the energy balance of heart muscle. Annu Rev Physiol 36: 413–459

Park S, Jeon JH, Min BK, Ha CM, Thoudam T, Park BY, Lee IK (2018) Role of the pyruvate dehydrogenase complex in metabolic remodeling: differential pyruvate dehydrogenase complex functions in metabolism. Diabetes Metab J 42: 270–281

Peng F, Wang JH, Fan WJ, Meng YT, Li MM, Li TT, Cui B, Wang HF, Zhao Y, An F et al (2018) Glycolysis gatekeeper PDK1 reprograms breast cancer stem cells under hypoxia. Oncogene 37: 1062–1074

Perez-Riverol Y, Csordas A, Bai J, Bernal-Llinares M, Hewapathirana S, Kundu DJ, Inuganti A, Griss J, Mayer G, Eisenacher M et al (2019) The PRIDE database and related tools and resources in 2019: improving support for quantification data. Nucleic Acids Res 47: D442–D450

Piquereau J, Ventura-Clapier R (2018) Maturation of cardiac energy metabolism during perinatal development. Front Physiol 9: 1–10

Poss KD, Wilson LG, Keating MT (2002) Heart regeneration in zebrafish. Science 298: 2188–2190

Puente BN, Kimura W, Muralidhar SA, Moon J, Amatruda JF, Phelps KL, Grinsfelder D, Rothermel BA, Chen R, Garcia JA et al (2014) The oxygen-rich postnatal environment induces cardiomyocyte cell-cycle arrest through DNA damage response. Cell 157: 565–579

Rappsilber J, Ishihama Y, Mann M (2003) Stop and go extraction tips for matrix-assisted laser desorption/ionization, nanoelectrospray, and LC/MS sample pretreatment in proteomics. Anal Chem 75: 663–670

Rardin MJ, Wiley SE, Naviaux RK, Murphy AN, Dixon JE (2009) Monitoring phosphorylation of the pyruvate dehydrogenase complex. Anal Biochem 389: 157–164

Ritchie ME, Phipson B, Wu D, Hu Y, Law CW, Shi W, Smyth GK (2015) Limma powers differential expression analyses for RNA-sequencing and microarray studies. Nucleic Acids Res 43: e47

Sallin P, de Preux Charles AS, Duruz V, Pfefferli C, Jazwinska A (2015) A dual epimorphic and compensatory mode of heart regeneration in zebrafish. Dev Biol 399: 27–40

Schindler YL, Garske KM, Wang J, Firulli BA, Firulli AB, Poss KD, Yelon D (2014) Hand2 elevates cardiomyocyte production during zebrafish heart development and regeneration. *Development* 141: 3112–3122

Shevchenko A, Tomas H, Havlis J, Olsen JV, Mann M (2006) In-gel digestion for mass spectrometric characterization of proteins and proteomes. *Nat Protoc* 1: 2856–2860

Stone OA, El-Brolosy M, Wilhelm K, Liu X, Romao AM, Grillo E, Lai JKH, Gunther S, Jeratsch S, Kuenne C *et al* (2018) Loss of pyruvate kinase M2 limits growth and triggers innate immune signaling in endothelial cells. *Nat Commun* 9: 4077

Tahara N, Brush M, Kawakami Y (2016) Cell migration during heart regeneration in zebrafish. *Dev Dyn* 245: 774–787

Takubo K, Nagamatsu G, Kobayashi CI, Nakamura-Ishizu A, Kobayashi H, Ikeda E, Goda N, Rahimi Y, Johnson RS, Soga T *et al* (2013) Regulation of glycolysis by Pdk functions as a metabolic checkpoint for cell cycle quiescence in hematopoietic stem cells. *Cell Stem Cell* 12: 49–61

Wagner KR, Max SR, Grollman EM, Koski CL (1976) Glycolysis in skeletal muscle regeneration. *Exp Neurol* 52: 40–48

Wang X, Ha T, Liu L, Hu Y, Kao R, Kalbfleisch J, Williams D, Li C (2018) TLR3 mediates repair and regeneration of damaged neonatal heart through glycolysis dependent YAP1 regulated miR-152 expression. *Cell Death Differ* 25: 966–982

Wilhelm K, Happel K, Eelen G, Schoors S, Oellerich MF, Lim R, Zimmermann B, Aspalter IM, Franco CA, Boettger T *et al* (2016) FOXO1 couples metabolic activity and growth state in the vascular endothelium. *Nature* 529: 216–220

Wu CC, Kruse F, Vasudevarao MD, Junker JP, Zebrowski DC, Fischer K, Noel ES, Grun D, Berezikov E, Engel FB *et al* (2016) Spatially resolved genome-wide transcriptional profiling identifies BMP signaling as essential regulator of zebrafish cardiomyocyte regeneration. *Dev Cell* 36: 36–49

Xie C, Mao X, Huang J, Ding Y, Wu J, Dong S, Kong L, Gao G, Li CY, Wei L (2011) KOBAS 2.0: a web server for annotation and identification of enriched pathways and diseases. *Nucleic Acids Res* 39: W316–W322

Zhang S, Hulver MW, McMillan RP, Cline MA, Gilbert ER (2014) The pivotal role of pyruvate dehydrogenase kinases in metabolic flexibility. *Nutr Metab* 11: 10 .

Zhao G, Jeoung NH, Burgess SC, Rosaaen-Stowe KA, Inagaki T, Latif S, Shelton JM, McAnally J, Bassel-Duby R, Harris RA *et al* (2008) Overexpression of pyruvate dehydrogenase kinase 4 in heart perturbs metabolism and exacerbates calcineurin-induced cardiomyopathy. *Am J Physiol Heart Circ Physiol* 294: H936–H943

Zheng X, Boyer L, Jin M, Mertens J, Kim Y, Ma L, Ma L, Hamm M, Gage FH, Hunter T (2016) Metabolic reprogramming during neuronal differentiation from aerobic glycolysis to neuronal oxidative phosphorylation. *eLife* 5: e13374